Proteomics Analysis of Cardiac Extracellular Matrix Remodeling in a Porcine Model of Ischemia-Reperfusion Injury

Running title: *Barallobre-Barreiro et al.; Cardiac extracellular matrix remodelling*

Javier Barallobre-Barreiro, MSc[1]; Athanasios Didangelos, PhD[2]; Friedrich A. Schoendube, MD[3]; Ignat Drozdov, PhD[2,4]; Xiaoke Yin, PhD[2]; Mariana Fernández-Caggiano, BSc[1]; Peter Willeit, MD[5]; Valentina O. Puntmann, MD, PhD[2]; Guillermo Aldama-López, MD[6]; Ajay M. Shah, MD, FMedSci[2]; Nieves Doménech, PhD[1]; Manuel Mayr, MD, PhD[2]

[1]Unidad de Investigación - INIBIC-CHU A Coruña, A Coruña, Spain; [2]Cardiovascular Division, King's British Heart Foundation Centre, King's College London, London, UK; [3]Faculty of Medicine, University of Goettingen, Goettingen, Germany; [4] Centre for Bioinformatics - School of Physical Sciences and Engineering, King's College London, London, UK; [5]Department of Public Health and Primary Care, University of Cambridge, Cambridge, UK; [6]Interventional Cardiology Unit, A Coruña University Hospital, A Coruña, Spain

Correspondence:

Manuel Mayr, MD, PhD

King's British Heart Foundation Centre

King's College London

125 Coldharbour Lane, London

SE5 9NU, UK

Phone: +44 (0) 20 7848 5132

Fax: +44 (0) 20 7848 5296

Email: manuel.mayr@kcl.ac.uk

Journal Subject Codes: [4] Acute myocardial infarction, [11] Other heart failure, [130] Animal models of human disease, [108] Other myocardial biology

Abstract:

Background - Following myocardial ischemia, extracellular matrix (ECM) deposition occurs at the site of the focal injury and at the border region.

Methods and Results - We have applied a novel proteomic method for the analysis of ECM in cardiovascular tissues to a porcine model of ischemia-reperfusion injury. ECM proteins were sequentially extracted and identified by liquid chromatography tandem mass spectrometry. For the first time, ECM proteins, such as cartilage intermediate layer protein 1 (CILP-1), matrilin-4, extracellular adipocyte enhancer binding protein 1 (AEBP-1), collagen alpha-1 (XIV) and several members of the small leucine-rich proteoglycan family, including asporin and prolargin, were shown to contribute to cardiac remodeling. A comparison in two distinct cardiac regions (the focal injury in the left ventricle and the border region close to the occluded coronary artery) revealed a discordant regulation of protein and messenger RNA levels: while gene expression for selected ECM proteins was similar in both regions, the corresponding protein levels were much higher in the focal lesion. Further analysis based on more than hundred ECM proteins delineated a signature of early and late stage cardiac remodelling with transforming growth factor beta 1 (TGFβ-1) signalling being at the centre of the interaction network. Finally, novel cardiac ECM proteins identified by proteomics were validated in human left ventricular tissue acquired from ischemic cardiomyopathy patients at cardiac transplantation.

Conclusions – Our findings reveal a bio-signature of early and late stage ECM remodeling after myocardial ischemia-reperfusion injury, which may have clinical utility as prognostic markers and modifiable targets for drug discovery.

Key words: cardiac remodeling; fibrosis; ischemic heart disease; matrix; proteomics

Introduction

Left ventricular (LV) remodeling after myocardial infarction is an important predictor of progression to heart failure and an early marker of increased morbidity and mortality[1]. Initiated by the loss of cardiomyocytes and cardiac function, the remodeling process is characterised by differentiation of cardiac fibroblasts into myofibrobasts, exhibiting secretory, proliferative and contractile functions in the post-injury state. Myofibroblasts contribute to the compensatory tissue replacement and interstitial fibrosis by effectively regulating the ECM turnover[2], primarily in the area of the focal injury but also in the border region[3-4]. Once initiated, the remodeling process is continuous, even after the initial injury has abated, leading to systolic and diastolic impairment. Furthermore, accumulation of collagen disrupts electrical coupling with increased arrhythmic susceptibility, and perivascular fibrosis impairs oxygen diffusion and exacerbates ongoing tissue ischemia and fibrosis[5]. Current anti-remodeling strategies targeting the renin-angiotensin-aldosteron system delay or prevent the development of heart failure largely by reducing the extent of interstitial collagen deposition[6]. Since fibrosis is probably reversible prior to the maladaptive changes of the collagen network and development of a mature scar[7-8], it is pertinent to characterise the different stages of ECM remodeling.

Thus far, proteomics studies were performed on whole heart tissue[9-10] or on subcellular fractions[11], including myofilaments[12], mitochondria[13], cytosolic[14] and nuclear extracts[15], but an in-depth analysis of the cardiac ECM has not been reported to date. The aim of the present study is to characterise ECM remodeling following myocardial infarction by applying a recently developed proteomics method[16] to a porcine model of ischemia-reperfusion (I/R) injury. Their human-like physiology and anatomy facilitates comparisons of different cardiac regions to establish an accurate temporal and spatial pattern of the ECM remodeling process.

Methods

An expanded Methods section is available in the Online Data Supplement at http://circ.ahajournals.org.

Porcine model of I/R injury

Nineteen three-month-old pigs were randomly assigned into the I/R (n=13) or the control group (Ctrl, n=6). Ischemia was induced by inserting an inflatable catheter and occluding the left anterior descending coronary artery for 120 min (see **Movie** in the **online Data Supplement**). All procedures followed the "European agreement of vertebrate animal protection for experimental use (86/609)".

Proteomic analysis

ECM proteins were extracted using an adaptation of a recently published method[16] and analysed by liquid chromatography tandem mass spectrometry as detailed in the online Data Supplement.

Human cardiac tissue

Cardiac tissue samples were obtained from patients undergoing cardiac transplantation at the A Coruña Hospital under approval from the Galician Ethics Committee for Research. Control tissues were obtained from unused donor hearts from the A Coruña Hospital following guidelines of Spanish Royal Decrees 2070/1999 and 1301/2006, which regulate the obtainment of human tissues for clinical and research purposes. Written informed consent was obtained from all patients.

Statistical analysis

Student's t-tests were used to compare protein expression between early and late fibrosis and control samples in the focal lesion and the border zone close to the coronary artery. False

Discovery Rates (FDR) were calculated using the R-package QVALUE with standard settings[17]. Protein spectral counts were log-transformed and z-transformed in an attempt to create data with normal distributions and increase the signal of low-abundant proteins. Z-score transformation of spectral counts was performed as follows: the expression measurement for each protein was adjusted to have a mean of 0 and a standard deviation of 1 across all conditions. Biological interpretation was based on relevant scientific literature[18]. Principal component analysis (PCA) was performed in Matlab version 2009a (The Mathworks Ltd). The 20 most significantly expressed proteins across all groups were identified based on one-way ANOVA. The effects of treatment (TGFβ, hypoxia, TGFβ + hypoxia) and time (24h, 48h) on ECM protein expression in cardiac fibroblasts were assessed by two-way ANOVAs followed by Bonferroni post tests. A P-value of <0.05 was considered significant.

Results

Porcine model of I/R injury

Pigs were subjected to I/R injury and sacrificed either 15 days (I/R15, n=9) or 60 days (I/R60, n=4) later. Six animals served as controls (Ctrl, **Supplemental Table 1**). Infarct development and location were confirmed by electrocardiogram (**Supplemental Figure 1**). LV function and size were assessed by echocardiography (**Figure 1A,** see supplemental **Movie**). The LV ejection fraction was 60.9±10.0% in controls compared to 34.3±10.3% in pigs at day 15 (means±SD, p=0.01) and 30.0±5.1% at day 60 (p=0.001) post injury. LV wall thickness was reduced from 11.4±1.8mm in controls to 6.6±2.5mm in the I/R 15 (means±SD, p<0.001) and to 5.6±2.1mm in the I/R 60 group (p<0.001). A representative macroscopic image is shown in **Figure 1B**. 15 days post I/R injury, cardiac tissue was sampled from two different regions: 1) the

border zone close to the coronary artery (I/R15 COR); 2) the focal lesion of the left ventricle (I/R15 LV), where the ischemic injury is most pronounced. Equivalent regions were sampled in controls (COR Ctrl and LV Ctrl). Four pigs were kept for 60 days after the operation to provide reference samples for late fibrosis (I/R60 LV). To visualize the extent of fibrosis, tissue sections were stained with Masson's trichrome. Counterstaining was performed with hematoxylin & eosin (**Figure 1C**).

Identification of extracellular proteins

Four animals per group (Ctrl, I/R15, and I/R60) were used for proteomics. Heart samples were consecutively incubated with 0.5M sodium chloride (NaCl), 0.1% sodium dodecyl sulfate (SDS) and 4M guanidine (Guanidine-HCl) to decellularize and sequentially extract extracellular space proteins[16]. The effectiveness of the decellularization procedure (SDS) was confirmed by electron microscopy (**Figure 2A**). The NaCl and Guanidine-HCl extracts were separated by SDS PAGE (**Supplemental Figure 2)**, the entire lane was divided into a series of gel bands and proteomic analysis was performed on each of them using a high mass accuracy tandem mass spectrometer (LTQ Orbitrap XL, ThermoFisher Scientific). In total, 139 extracellular space proteins **(Table 1)** were identified with minimum of 2 high confidence peptides (**Supplemental Table 2** and **3** for NaCl and Guanidine-HCl extracts, respectively). Among the identified proteins were 17 proteoglycans, 25 collagen subunits, and 84 glycoproteins, while the remaining 13 were proteins known to be associated with ECM, including apolipoproteins, proteases etc. As expected, NaCl extracts were enriched with proteins of the extracellular space and newly synthesised ECM proteins, which are not heavily cross-linked on the interstitial matrix. Guanidine-HCl extracts instead contained predominantly proteoglycans, glycoproteins and collagens (**Figure 2B**). Importantly, several proteins were identified for the first time in the

cardiac ECM (see footnote in **Table 1**). Representative MS/MS spectra of these proteins are provided in **Supplemental Figure 3**. Protein ambiguity was resolved using the Scaffold software and peptides assigned to more than one protein are highlighted in **Supplemental Table 4**. Peptide identifications for all ECM and ECM-associated proteins are provided in **Supplemental Table 5** and **6**.

Differential expression analysis

A comparison of protein changes during cardiac ECM remodelling was performed using label-free quantitation as previously described[12] (**Table 1).** Classic remodeling markers such as collagen type I and III were increased in both extracts indicating active ECM remodeling with continuous synthesis of ECM proteins (NaCl) and subsequent incorporation to the interstitial matrix (Guanidine-HCl). At 15 days, few ECM proteins changed significantly the border zone (I/R15 COR, **Figure 3A**), but pronounced changes were observed in the focal lesion (I/R15 LV, **Figure 3B**), i.e. for cartilage intermediate layer protein 1 (CILP-1), asporin (ASPN), adipocyte enhancer binding protein 1 (AEBP-1), and TGFβ-induced protein ig-h3 (BGH3). Cartilage and bone-related proteins, such as aggrecan (PGCA) and chondroadherin (CHAD), were only found at day 60 (**Figure 3C**). Notably, several of these proteins are downstream targets of TGFβ-1, a major pro-fibrotic factor (**Figure 4**). However, interactions for CILP-1, asporin or aggrecan had to be inferred from experiments on other tissues, i.e. cartilage, since these proteins are currently not in public cardiac matrix interaction databases.

Bioinformatic analysis

Principal component analyses were used for visual display of regional and temporal differences in the ECM post I/R injury (**Figure 5A** and **B** for NaCl and Guanidine-HCl extracts, respectively). The matrix profile of the border zone (I/R15 COR), the focal lesion (I/R15 LV)

and late fibrosis (I/R60 LV) was clearly distinct from the respective controls (COR Ctrl and LV Ctrl), suggesting a high reproducibility of our proteomic technique. Expression patterns of the top 20 most differentially expressed proteins across all samples (identified by one-way ANOVA) are shown in **Figure 5C** and **D** (NaCl and Guandine-HCl extracts, respectively). Expression changes covering different groups of ECM proteins were selected for further validation and are highlighted in the Figure.

Validation

Using real-time PCR, an induction of CILP1, asporin, aortic carboxipeptidase (ACLP - the extracellular isoform of AEBP-1), BGH3, collagen XIV (COEA1) and XVIII (COIA1) was confirmed (**Figure 6A)** in the same tissue specimen used for proteomic analysis (**Figure 6B, C**). While the messenger RNA levels of these ECM components were highly correlated in the focal (I/R15 LV) and the border (I/R15 COR) region (**Figure 6D**), the spectral counts for the corresponding proteins were markedly higher in the focal lesion (**Figure 6E**). We confirmed the upregulation of asporin, dermatopontin, ACLP/AEBP-1, biglycan and periostin in the infarcted LV by immunoblotting (**Figure 7A**). In contrast, the inactive latency associated peptide-TGFβ-1 complex was reduced (**Figure 7A, B**), suggesting that most of the TGFβ-1 present within cardiac tissue is bioactive after I/R injury, which is consistent with the upregulation of thrombospondin 1 (**Table 1**), the most potent activator of TGFβ-1 signalling[19]. Indeed, TGFβ-1 but not hypoxia induced the expression of BGH3 and dermatopontin in isolated pig cardiac fibroblasts (**Figure 7C**). Induction of asporin was observed after a combined stimulation by hypoxia and TGFβ-1. Expression levels for ACLP/AEBP-1 remained similar to controls. In agreement with this finding, positive staining for ACLP/AEBP-1 in LV tissue was predominantly observed intracellular in cardiomyocytes rather than cardiac fibroblasts. In contrast, periostin, which is

expressed within cardiac fibroblasts in response to exogenous TGFβ-1 but not in cardiomyocytes[20], revealed a distinct extracellular distribution pattern (**Figure 7D**). Weaker extra- and pericellular immunostaining was apparent for dermatopontin and BGH3. Finally, the presence of novel cardiac ECM proteins was validated in patients undergoing cardiac transplant surgery for ischemic heart failure. Clinical characteristics are provided in **Supplemental Table 7**. For each patient, representative tissue sections are shown in **Supplemental Figure 4**. Immunofluorescence staining for CILP, asporin and dermatopontin was seen in ischemic porcine (I/R15 LV, **Figure 8A**) as well as human LV tissue (**Figure 8B**).

Discussion

There are several important aspects to this study. First, by diverging from the traditional focus on intracellular proteins, we employed a sequential extraction procedure in combination with state of the art proteomics. By using this conceptually novel approach, our findings reveal previously unknown cardiac ECM components and provide important insights into ECM remodeling, by region and stage of fibrosis. The extensive proteomic comparison allowed for the first time a co-expression analysis of ECM proteins during early and late stages of cardiac remodeling.

A proteomics approach for ECM

Thus far, proteomics studies investigating cardiac diseases have been focused on intracellular proteins, with little emphasis on ECM and proteins in the extracellular space. To overcome the bias towards the cellular proteome and the failure to detect cardiac ECM proteins in proteomics analysis, we have applied a novel method optimized for the analysis of cardiac ECM[16]: This method is based on decellularisation and a sequential extraction procedure to enrich

for ECM components. It provides a simplified subproteome abundant in matrix proteins that can be interrogated by label-free quantification. This is important because no proteomic technology can currently resolve the entire complexity of the mammalian proteome, and there is a trade-off between sensitivity and quantitative accuracy. Previous quantitative comparisons applying shotgun proteomics to cardiac tissue had to exclude fractions containing myofilament proteins in order to alleviate the severe dynamic range limitations stemming from highly abundant contractile components[14]. Similarly, in our method the decellularisation step is essential to improve sensitivity and quantitative accuracy in the ECM subproteome[16]. Unlike any other cardiac proteomics study published to date, newly synthesised matrix proteins or loosely bound factors in the extracellular space were extracted before the tissues were decellularised[21]. Then, integral ECM components, such as proteoglycans, glycoproteins or cross-linked collagens, which are not dissolved in conventional extraction buffers, were solubilised under harsh conditions.

Advantages of proteomics

The primary ECM deposited after myocardial infarction is composed of fibrin and plasma-derived fibronectin, which serves as the initial scaffold for the migration and expansion of fibroblasts as well as the infiltration of inflammatory cells before a more definitive ECM is synthesised with newly formed matrix components[22-23]. Trancriptomics provides valuable insights regarding the expression and regulation of ECM proteins at the mRNA level. ECM-associated proteins, however, which are not expressed by cardiac cells but are plasma-derived, remain undetected. Moreover, microarrays only provide a snapshot of mRNA expression at a particular time point. In contrast, proteomics measures the actual ECM that has accumulated over time as net effect of protein synthesis and protein degradation. In comparison to conventional antibody-based techniques, a proteomics screening method is better suited to

capture the complex interactions during ECM remodelling, but it cannot reveal the spatial localisation of these ECM proteins within the cardiac tissue. In our study, the ischemic injury and the subsequent fibrosis were less pronounced in the border region compared to the focal lesion. At the time of harvest, however, gene expression of selected ECM proteins was similar in the two regions suggesting that a pro-fibrotic programme had been initiated in both areas. Gene transcripts have a much shorter half-life than proteins and a stable protein is not necessarily encoded by a stable mRNA. Moreover, ECM remodelling is subject to an intricate network of control, including microRNAs for translational repression. This lack of correlation between protein and mRNA levels demonstrates the complementary nature of transcriptomics and proteomics in studying cardiac ECM remodelling.

The importance of ECM in cardiac remodelling

Myocardial fibrosis is a hallmark of cardiac remodeling in response to ischemia, and closely linked with arrhythmogenicity and impairment of both systolic and diastolic function. Although cardiomyocytes constitute 70% of the cardiac tissue mass, they only represent about one third of the cells. The other predominant cell type within the heart muscle is the fibroblast[5]. Fibroblasts actively synthesise and secrete ECM, and also contribute to the propagation of the electrical signals that orchestrate cardiac contraction[24]. In disease, the transition of fibroblasts to myofibroblasts, regulated in part by TGFβ-1, induces a pro-fibrotic state that contributes to cardiac dysfunction with consequent impairment of contractile properties and relaxation, and rhythm disturbance by affecting electrical signal propagation and arrhythmogenicity[25]. The cardiac ECM not only provides structural support, but also retains soluble growth factors and regulates their distribution[26]. For example, fibroblast growth factor and vascular endothelial growth factor bind avidly to the heparan sulfate component of many ECM proteoglycans.

Growth factors also bind to ECM proteins themselves, without the involvement of glycosaminoglycans, i.e. vascular endothelial growth factor binds to specific fibronectin type III domains present in both fibronectin and tenascin-C supporting the notion that the presentation of growth factor signals by ECM proteins is an important part of ECM function[26]. As such, a comprehensive description of the ECM is essential to decipher the complex, multivalent signals that are presented to cells during cardiac remodeling.

Novel downstream targets of TGFβ-1

TGFβ is a critical pro-fibrotic molecule in the heart[23], but some of its downstream targets identified in this study have either never been reported in cardiac tissue thus far or not been studied in the context of cardiac remodeling. For example, CILP1 was described as a cartilage protein[27]. It contains thrombospondin type I repeats that potentially modulate its anchoring ability to other ECM components, including glycosaminoglycans and interestingly, TGFβ-1[28-29]. In our proteomics analysis, the highest levels of CILP1 were observed in the focal lesion 15 days post I/R injury, where CILP1 may act by antagonizing TGFβ-1 as reported by studies in other tissues[30]. Similarly, asporin is a critical regulator of TGFβ-1 in articular cartilage. It blocks the interaction of TGFβ-1 with the TGFβ type II receptor[31-32] on the cell surface and inhibits the canonical TGFβ-1/Smad signalling pathway. Yet, the presence of neither CILP1 nor asporin has been demonstrated in cardiac tissue at the protein level. Other modulators of TGFβ-1 signalling have not been studied in the context of cardiac remodeling: Dermatopontin enhances TGFβ−1 activity, accelerates collagen fibril formation, and stabilizes collagens[33]. BGH3 is an extracellular reporter of TGFβ−1 activity[34]. It serves as a communication link between fibroblasts and its ECM environment by mediating adhesion via integrin binding and inhibits cell

proliferation[35]. Also, the presence of the cartilage protein aggrecan has only been reported in hearts of developing chicken embryos[36], but further studies in adult cardiac tissue have not been performed thus far. Thus, our study will serve as an important reference for future investigations exploring the function of these novel proteins and developing transgenic animal models to study their contribution to the cardiac remodeling process.

Conclusions

Using a porcine model of I/R injury and state-of-the-art mass spectrometry, we provide the first proteomic characterisation of cardiac ECM remodeling. This innovative strategy allowed novel insights, which may be useful for early detection of adverse remodeling events and predicting the likelihood of the occurrence of heart failure. For example, characteristic changes for early and late fibrosis could be monitored by molecular imaging techniques over the course of disease or in response to therapy to personalize its delivery.

Funding Sources: J.B.B. is supported by grants from CHU A Coruña Foundation and Xunta de Galicia. I.D. is supported by a PhD studentship from the British Heart Foundation. M.M. is a Senior Research Fellow of the British Heart Foundation.

Conflict of Interest Disclosures: None

References:

1. Pfeffer MA, Braunwald E. Ventricular remodeling after myocardial infarction. Experimental observations and clinical implications. *Circulation.* 1990;81:1161–1172.

2. van den Borne SW, Diez J, Blankesteijn WM, Verjans J, Hofstra L, Narula J. Myocardial remodeling after infarction: the role of myofibroblasts. *Nat Rev Cardiol.* 2010;7:30-37.

3. Volders PG, Willems IE, Cleutjens JP, Arends JW, Havenith MG, Daemen MJ. Interstitial collagen is increased in the non-infarcted human myocardium after myocardial infarction. *J Mol Cell Cardiol*. 1993;25:1317–1323.

4. Sutton MG, Sharpe N. Left ventricular remodeling after myocardial infarction: pathophysiology and therapy. *Circulation.* 2000;101:2981-2988.

5. Baudino TA, Carver W, Giles W, Borg TK. Cardiac fibroblasts: friend or foe? *Am J Physiol Heart Circ Physiol.* 2006;291:H1015-H1026.

6. Cleutjens JP, Blankesteijn WM, Daemen MJ, Smits JF. The infracted myocardium: simply dead tissue, or a lively target for therapeutic interventions. *Cardiovasc Res.* 1999;44:232–241.

7. Berk BC, Fujiwara K, Lehoux S. ECM remodeling in hypertensive heart disease. *J Clin Invest.* 2007;117:568-575.

8. van den Borne SW, Isobe S, Zandbergen HR, Li P, Petrov A, Wong ND, Fujimoto S, Fujimoto A, Lovhaug D, Smits JF, Daemen MJ, Blankesteijn WM, Reutelingsperger C, Zannad F, Narula N, Vannan MA, Pitt B, Hofstra L, Narula J.Molecular imaging for efficacy of pharmacologic intervention in myocardial remodeling. *JACC Cardiovasc Imaging.* 2009;2:187-198.

9. Cieniewski-Bernard C, Mulder P, Henry JP, Drobecq H, Dubois E, Pottiez G, Thuillez C, Amouyel P, Richard V, Pinet F. Proteomic analysis of left ventricular remodeling in an experimental model of heart failure. *J Proteome Res.* 2008;7:5004-5016.

10. Mayr M, Yusuf S, Weir G, Chung YL, Mayr U, Yin X, Ladroue C, Madhu B, Roberts N, De Souza A, Fredericks S, Stubbs M, Griffiths JR, Jahangiri M, Xu Q, Camm AJ. Combined metabolomic and proteomic analysis of human atrial fibrillation. *J Am Coll Cardiol.* 2008;51:585-594.

11. Arrell DK, Neverova I, Van Eyk JE. Cardiovascular proteomics: evolution and potential. *Circ Res.* 2001;88:763-773.

12. Yin X, Cuello F, Mayr U, Hao Z, Hornshaw M, Ehler E, Avkiran M, Mayr M. Proteomics analysis of the cardiac myofilament subproteome reveals dynamic alterations in phosphatase subunit distribution. *Mol Cell Proteomics.* 2010;9:497-509.

13. Mayr M, Liem D, Zhang J, Li X, Avliyakulov NK, Yang JI, Young G, Vondriska TM, Ladroue C, Madhu B, Griffiths JR, Gomes A, Xu Q, Ping P. Proteomic and metabolomic analysis of cardioprotection: Interplay between protein kinase C epsilon and delta in regulating glucose metabolism of murine hearts. *J Mol Cell Cardiol*. 2009;46:268-277.

14. Gramolini AO, Kislinger T, Alikhani-Koopaei R, Fong V, Thompson NJ, Isserlin R, Sharma P, Oudit GY, Trivieri MG, Fagan A, Kannan A, Higgins DG, Huedig H, Hess G, Arab S, Seidman JG, Seidman CE, Frey B, Perry M, Backx PH, Liu PP, MacLennan DH, Emili A.

Comparative proteomics profiling of a phospholamban mutant mouse model of dilated cardiomyopathy reveals progressive intracellular stress responses. *Mol Cell Proteomics.* 2008;7:519-533.

15. Franklin S, Zhang MJ, Chen H, Paulsson AK, Mitchell-Jordan SA, Li Y, Ping P, Vondriska TM. Specialized compartments of cardiac nuclei exhibit distinct proteomic anatomy. *Mol Cell Proteomics.* 2011;10:M110.000703. Epub 2010 Aug 31.

16. Didangelos A, Yin X, Mandal K, Baumert M, Jahangiri M, Mayr M. Proteomic characterization of extracellular space components in the human aorta. *Mol Cell Proteomics.* 2010;9:2048-2062.

17. Storey JD, Tibshirani R. Statistical significance for genomewide studies. *Proc Natl Acad Sci U S A.* 2003;100:9440-9445.

18. Cheadle C, Vawter MP, Freed WJ, Becker KG. Analysis of microarray data using Z score transformation. *J Mol Diagn.* 2003;5:73-81.

19. Schellings MW, van Almen GC, Sage EH, Heymans S. Thrombospondins in the heart: potential functions in cardiac remodeling. *J Cell Commun Signal.* 2009;3:201-213.

20. Snider P, Hinton RB, Moreno-Rodriguez RA, Wang J, Rogers R, Lindsley A, Li F, Ingram DA, Menick D, Field L, Firulli AB, Molkentin JD, Markwald R, Conway SJ. Periostin is required for maturation and extracellular matrix stabilization of noncardiomyocyte lineages of the heart. *Circ Res.*2008;102:752-760.

21. Ott HC, Matthiesen TS, Goh SK, Black LD, Kren SM, Netoff TI, Taylor DA. Perfusion-decellularized matrix: using nature's platform to engineer a bioartificial heart. *Nat Med.* 2008;14:213-221.

22. McCurdy S, Baicu CF, Heymans S, Bradshaw AD. Cardiac extracellular matrix remodeling: fibrillar collagens and Secreted Protein Acidic and Rich in Cysteine (SPARC). *J Mol Cell Cardiol.* 2010;48:544-549.

23. Dobaczewski M, Gonzalez-Quesada C, Frangogiannis NG. The extracellular matrix as a modulator of the inflammatory and reparative response following myocardial infarction. *J Mol Cell Cardiol*. 2010;48:504-511.

24. Kohl P, Camelliti P, Burton FL, Smith GL. Electrical coupling of fibroblasts and myocytes: relevance for cardiac propagation. *J Electrocardiol.* 2005;38:45-50.

25. Leask A. Potential therapeutic targets for cardiac fibrosis: TGFbeta, angiotensin, endothelin, CCN2, and PDGF, partners in fibroblast activation. *Circ Res.* 2010;106:1675-1680.

26. Hynes RO. The extracellular matrix: not just pretty fibrils. *Science.* 2009;326:1216-1219.

27. Lorenzo P, Neame P, Sommarin Y, Heinegård D. Cloning and deduced amino acid sequence of a novel cartilage protein (CILP) identifies a proform including a nucleotide pyrophosphohydrolase. *J Biol Chem.* 1998;273:23469-23475.

28. Johnson K, Farley D, Hu SI, Terkeltaub R. One of two chondrocyte-expressed isoforms of cartilage intermediate-layer protein functions as an insulin-like growth factor 1 antagonist. *Arthritis Rheum*. 2003;48:1302-1314.

29. Yao Z, Nakamura H, Masuko-Hongo K, Suzuki-Kurokawa M, Nishioka K, Kato T. Characterisation of cartilage intermediate layer protein (CILP)-induced arthropathy in mice. *Ann Rheum Dis.* 2004;63:252-258.

30. Seki S, Kawaguchi Y, Chiba K, Mikami Y, Kizawa H, Oya T, Mio F, Mori M, Miyamoto Y, Masuda I, Tsunoda T, Kamata M, Kubo T, Toyama Y, Kimura T, Nakamura Y, Ikegawa S.A functional SNP in CILP, encoding cartilage intermediate layer protein, is associated with susceptibility to lumbar disc disease. *Nat Genet.* 2005;37:607-612.

31. Kou I, Nakajima M, Ikegawa S. Binding characteristics of the osteoarthritis-associated protein asporin. *J Bone Miner Metab.* 2010;28:395-402.

32. Nakajima M, Kizawa H, Saitoh M, Kou I, Miyazono K, Ikegawa S. Mechanisms for asporin function and regulation in articular cartilage. *J Biol Chem.* 2007;282:32185-32192.

33. Okamoto O, Fujiwara S. Dermatopontin, a novel player in the biology of the extracellular matrix. *Connect Tissue Res.* 2006;47:177-189.

34. Langham RG, Egan MK, Dowling JP, Gilbert RE, Thomson NM. Transforming growth factor-beta1 and tumor growth factor-beta-inducible gene-H3 in nonrenal transplant cyclosporine nephropathy. *Transplantation.* 2001;72:1826-1829.

35. Thapa N, Kang KB, Kim IS. Beta ig-h3 mediates osteoblast adhesion and inhibits differentiation. *Bone.* 2005;36:232-242.

36. Zanin MK, Bundy J, Ernst H, Wessels A, Conway SJ, Hoffman S. Distinct spatial and temporal distributions of aggrecan and versican in the embryonic chick heart. *Anat Rec.* 1999;256:366-380.

Table 1. ECM Remodeling in a Porcine Model of I/R Injury.

Protein		NaCl extract						Guanidine-HCl extract					
		COR I/R15 vs COR Ctrl		LV I/R15 vs LV Ctrl		LV I/R60 vs LV Ctrl		COR I/R15 vs COR Ctrl		LV I/R15 vs LV Ctrl		LV I/R60 vs LV Ctrl	
Accession number	Full name	Fold change	P value	Fold change	P value	Fold change	P value	Fold change	P value	Fold change	P value	Fold change	P value
ADA11_HUMAN	ADAM 11							1.0	-	0.6	N/A	0.6	N/A
AEBP1_HUMAN	Adipocyte enhancer-binding protein 1 (ACLP)	1.3	N/A	18.3	0.003	18.0	0.002*	1.0	-	16.6	0.134	19.8	0.202
AGRIN_HUMAN	Agrin‡	0.5	0.035	3.0	0.058	1.0	-	0.5	0.246	2.7	0.095	0.8	0.656
AIBP_PIG	Apolipoprotein A-I-binding protein	0.7	0.203	0.3	0.029	0.3	0.029						
ANXA2_PIG	Annexin A2	1.8	0.007	1.6	0.043	1.7	0.015	2.4	0.155	15.4	0.002*	10.5	0.216
APOA1_PIG	Apolipoprotein A-I	1.6	0.020	1.4	0.016	1.7	0.032	1.3	0.536	3.4	0.023	5.9	0.261
APOA4_PIG	Apolipoprotein A-IV	3.0	<0.001*	10.7	0.026	23.0	0.012	1.0	-	1.0	-	13.0	0.269
APOB_HUMAN	Apolipoprotein B-100	0.4	0.001*	0.8	N/A	1.1	0.861	0.7	N/A	1.0	-	1.4	N/A
APOC3_PIG	Apolipoprotein C-III	2.0	N/A	1.8	N/A	1.0	-						
APOE_PIG	Apolipoprotein E	1.0	-	2.5	0.137	2.3	N/A	1.0	-	11.1	0.134	22.8	0.257
APOH_HUMAN	Beta-2-glycoprotein 1	1.0	-	1.0	-	3.0	N/A						
APOL4_HUMAN	Apolipoprotein L4	0.7	N/A	1.0	-	1.0	-						
APOM_HUMAN	Apolipoprotein M	1.0	-	1.5	N/A	1.0	-						
APOO_HUMAN	Apolipoprotein O							0.4	0.134	0.7	0.593	0.6	0.472
APOR_PIG	Apolipoprotein R							1.0	-	3.7	0.136	2.4	N/A
ASPN_HUMAN	Asporin‡							4.0	0.028	20.5	0.001*	15.1	<0.001*
ATS20_HUMAN	A disintegrin and metalloproteinase with thrombospondin motifs 20							1.2	0.739	1.0	-	1.0	-
ATS3_HUMAN	A disintegrin and metalloproteinase with thrombospondin motifs 3							1.0	-	0.6	N/A	0.6	N/A
ATS8_HUMAN	A disintegrin and metalloproteinase with thrombospondin motifs 8	0.6	0.154	1.0	-	1.0	-						
ATS9_HUMAN	A disintegrin and metalloproteinase with thrombospondin motifs 9	0.8	N/A	1.0	-	1.0	-	2.0	N/A	1.0	-	1.0	-
BGH3_PIG	Transforming growth factor-beta-induced protein ig-h3	5.4	0.131	9.8	0.187	7.5	0.114	4.4	0.067	23.4	0.004	7.4	<0.001*
CBPA1_HUMAN	Carboxypeptidase A1	1.0	-	1.2	N/A	1.0	-						
CH3L1_PIG	Chitinase-3-like protein 1	1.0	-	1.0	-	2.1	N/A						
CHAD_HUMAN	Chondroadherin	1.0	-	2.3	0.252	4.4	0.001*						
CHADL_HUMAN	Chondroadherin-like protein							0.5	0.134	1.5	N/A	1.0	-
CILP1_HUMAN	Cartilage intermediate layer protein 1‡	6.1	0.027	10.3	0.006	8.2	0.032	7.6	0.038	30.5	<0.001*	11.6	<0.001*
CILP2_HUMAN	Cartilage intermediate layer protein 2							1.8	N/A	1.0	-	1.0	-
CLUS_PIG	Clusterin	1.4	N/A	3.8	0.005	9.9	0.010	1.0	-	17.4	0.051	15.8	N/A
CO1A1_HUMAN	Collagen alpha-1(I)	2.5	0.138	4.7	0.001*	6.8	0.006	1.9	0.003	4.0	<0.001*	3.8	0.023
CO1A2_HUMAN	Collagen alpha-2(I)	2.7	N/A	5.2	0.162	11.0	0.005	1.5	N/A	2.2	0.146	2.9	N/A
CO2A1_HUMAN	Collagen alpha-1(II)							1.5	N/A	1.0	-	1.0	-
CO3A1_HUMAN	Collagen alpha-1(III)	4.5	0.068	4.5	0.001*	9.3	<0.001*	1.0	-	6.0	0.002*	6.5	0.124
CO4A1_HUMAN	Collagen alpha-1(IV)	1.0	-	1.0	-	1.3	N/A	0.7	N/A	3.6	N/A	4.1	0.064
CO4A2_HUMAN	Collagen alpha-2(IV)‡	1.0	-	2.7	0.164	1.0	-	0.7	N/A	10.4	0.134	4.8	N/A
CO4A3_HUMAN	Collagen alpha-3(IV)							1.5	N/A	1.0	-	1.0	-
CO4A4_HUMAN	Collagen alpha-4(IV)	1.2	N/A	1.0	-	1.0	-	1.0	-	0.6	N/A	0.6	N/A
CO5A1_HUMAN	Collagen alpha-1(V)	1.0	-	1.0	-	2.0	N/A	1.0	-	1.7	N/A	5.4	N/A
CO5A2_HUMAN	Collagen alpha-2(V)	1.0	-	1.0	-	1.7	N/A	2.6	N/A	4.8	N/A	9.7	<0.001*
CO5A3_HUMAN	Collagen alpha-3(V)							1.5	N/A	2.0	0.134	2.3	0.152
CO6A1_HUMAN	Collagen alpha-1(VI)	0.9	0.915	2.2	0.086	1.0	0.987	0.8	0.455	2.5	0.128	0.9	0.738
CO6A2_HUMAN	Collagen alpha-2(VI)	1.3	0.670	1.6	0.409	2.7	0.100	0.8	0.319	1.5	0.342	1.0	0.870
CO6A3_HUMAN	Collagen alpha-3(VI)	0.7	0.499	3.4	0.002*	2.1	0.181	0.9	0.814	3.6	0.067	1.2	0.466
CO6A5_HUMAN	Collagen alpha-5(VI)	1.0	-	1.0	-	1.0	-						
CO6A6_HUMAN	Collagen alpha-6(VI)	1.0	-	1.0	-	1.0	-	1.0	-	1.0	0.921	0.6	N/A
CO7A1_HUMAN	Collagen alpha-1(VII)	0.8	0.445	1.0	0.943	2.1	0.113	0.7	0.482	1.0	-	1.7	N/A
CO9A2_HUMAN	Collagen alpha-2(IX)	1.0	-	1.0	-	1.2	N/A						
COBA2_HUMAN	Collagen alpha-2(XI)							1.5	N/A	1.0	-	1.0	-

COCA1_HUMAN	Collagen alpha-1(XII)‡	5.3	0.034	25.5	0.001*	53.0	0.008	1.0	-	3.0	N/A	9.8	0.090
CODA1_HUMAN	Collagen alpha-1(XIII)							1.0	-	1.0	-	1.8	N/A
COEA1_HUMAN	Collagen alpha-1(XIV)‡	2.4	0.042	2.2	<0.001*	4.2	<0.001*	1.0	-	11.1	0.047	20.3	0.007
COFA1_HUMAN	Collagen alpha-1(XV)	0.6	0.178	2.7	0.136	1.7	N/A	0.4	0.158	5.7	0.131	1.6	0.607
COGA1_HUMAN	Collagen alpha-1(XVI)							1.8	N/A	2.2	N/A	4.5	0.036
COIA1_HUMAN	Collagen alpha-1(XVIII)	1.3	N/A	3.1	0.062	3.8	0.298	7.7	0.047	20.1	0.049	9.4	N/A
COKA1_HUMAN	Collagen alpha-1(XX)	1.0	-	0.8	N/A	0.8	N/A						
COMA1_HUMAN	Collagen alpha-1(XXII)							1.0	-	1.5	N/A	1.9	N/A
COMP_HUMAN	Cartilage oligomeric matrix protein	1.0	-	1.0	-	3.4	0.149						
COOA1_HUMAN	Collagen alpha-1(XXIV)							1.0	-	1.0	-	2.1	N/A
CPXM2_HUMAN	Carboxypeptidase-like protein X2	1.0	-	1.0	-	1.5	N/A						
CSPG2_HUMAN	Versican core protein	5.3	0.016	6.6	0.017	7.7	<0.001*	4.3	0.032	61.7	0.009	53.0	0.017
CTGF_PIG	Connective tissue growth factor							1.0	-	1.0	-	1.5	N/A
DAG1_PIG	Dystroglycan (Fragment)							1.7	N/A	1.0	-	1.0	-
DERM_PIG	Dermatopontin	1.0	-	3.7	0.028	5.3	0.001*	1.4	0.404	4.1	0.020	3.4	0.005
EMIL1_HUMAN	EMILIN-1‡							1.0	-	3.6	0.137	3.6	N/A
EMIL2_HUMAN	EMILIN-2							1.0	-	1.0	-	1.5	N/A
EMIL3_HUMAN	EMILIN-3							1.0	-	0.4	0.139	0.4	0.139
FBLN1_HUMAN	Fibulin-1	1.0	-	6.4	0.013	4.9	0.074						
FBLN2_HUMAN	Fibulin-2	0.8	N/A	6.5	0.038	3.0	0.155						
FBLN3_HUMAN	EGF-containing fibulin-like extracellular matrix protein 1	1.0	-	4.2	0.159	5.3	0.040						
FBLN4_HUMAN	EGF-containing fibulin-like extracellular matrix protein 2	1.0	-	1.0	-	2.2	N/A						
FBLN5_HUMAN	Fibulin-5	1.0	-	4.3	<0.001*	9.7	0.005						
FBN1_PIG	Fibrillin-1	1.0	-	1.8	0.187	1.0	-	1.7	N/A	2.2	N/A	8.2	0.301
FBN2_HUMAN	Fibrillin-2							1.0	-	1.0	-	1.5	N/A
FETUA_PIG	Alpha-2-HS-glycoprotein (Fragment)							1.7	N/A	4.1	0.149	15.1	N/A
FGF11_HUMAN	Fibroblast growth factor 11							2.1	N/A	1.0	-	1.0	-
FGF23_HUMAN	Fibroblast growth factor 23							1.0	-	0.6	N/A	0.6	N/A
FINC_HUMAN	Fibronectin	1.0	-	13.9	0.163	12.5	0.243	0.7	0.581	36.5	0.068	21.3	0.108
FMOD_HUMAN	Fibromodulin	1.6	N/A	6.7	0.003	9.8	<0.001*	1.9	N/A	8.0	0.135	14.0	0.136
FNDC1_HUMAN	Fibronectin type III domain-containing protein 1							1.0	-	1.5	N/A	1.0	-
FRAS1_HUMAN	Extracellular matrix protein FRAS1	0.8	N/A	1.2	N/A	1.0	-	1.0	-	1.0	-	1.5	N/A
FREM3_HUMAN	FRAS1-related extracellular matrix protein 3							0.7	N/A	1.0	-	1.0	-
GPC6_HUMAN	Glypican-6	1.0	-	1.2	N/A	1.0	-						
HMCN1_HUMAN	Hemicentin-1							1.1	0.917	1.0	-	1.0	-
IBP7_HUMAN	Insulin-like growth factor-binding protein 7							2.3	0.148	3.6	0.136	2.9	0.195
LAMA1_HUMAN	Laminin subunit alpha-1	0.8	N/A	1.0	-	1.6	N/A						
LAMA2_HUMAN	Laminin subunit alpha-2	0.2	0.030	0.2	<0.001*	0.1	<0.001*	0.1	0.046	1.3	0.608	0.1	0.046
LAMA4_HUMAN	Laminin subunit alpha-4	1.0	-	1.4	0.575	0.6	N/A	1.2	0.848	11.9	0.054	4.3	N/A
LAMA5_HUMAN	Laminin subunit alpha-5	1.3	N/A	1.2	N/A	1.0	-	1.0	-	6.8	0.116	2.3	0.159
LAMB1_HUMAN	Laminin subunit beta-1	0.4	0.177	0.4	0.003	0.2	<0.001*	0.2	0.002*	1.6	0.337	0.6	0.400
LAMB2_HUMAN	Laminin subunit beta-2	0.7	N/A	1.0	0.963	0.9	0.743	0.4	0.029	0.9	0.763	0.2	0.006
LAMB3_HUMAN	Laminin subunit beta-3	1.0	-	1.0	-	1.7	N/A	1.0	-	1.7	N/A	1.0	-
LAMC1_HUMAN	Laminin subunit gamma-1	0.5	0.080	0.6	0.031	0.4	0.002*	0.8	0.373	1.6	0.309	0.3	0.054
LAMC3_HUMAN	Laminin subunit gamma-3							1.0	-	1.0	-	1.4	N/A
LEG1_PIG	Galectin-1	1.1	0.626	1.9	0.006	1.0	0.869	2.3	N/A	14.0	0.001*	11.4	0.005
LEG3_HUMAN	Galectin-3	1.0	-	1.2	N/A	1.0	-	1.0	-	4.6	0.145	2.4	N/A
LTB1L_HUMAN	Latent-transforming growth factor beta-binding protein isoform 1L							1.8	N/A	1.0	-	1.0	-
LTB1S_HUMAN	Latent-transforming growth factor beta-binding protein isoform 1S	1.0	-	1.2	N/A	1.0	-	1.0	-	1.0	-	2.9	N/A
LTBP2_HUMAN	Latent-transforming growth factor beta-binding protein 2	1.0	-	2.2	N/A	1.7	N/A						
LTBP3_HUMAN	Latent-transforming growth factor beta-binding protein 3							1.0	-	1.5	N/A	1.0	-
LTBP4_HUMAN	Latent-transforming growth factor beta-binding protein 4	1.0	-	1.2	N/A	1.0	-						
LUM_HUMAN	Lumican	1.0	-	0.6	N/A	2.8	0.247	1.5	0.709	4.6	0.014	7.5	0.006
MATN2_HUMAN	Matrilin-2	1.0	-	1.5	0.526	1.4	0.583	1.5	N/A	1.7	N/A	1.0	-
MATN4_HUMAN	Matrilin-4‡	1.0	-	4.2	0.227	1.9	N/A	1.0	-	7.3	0.136	1.0	-
MFGM_PIG	Lactadherin							1.0	-	1.0	-	2.7	N/A
MGP_HUMAN	Matrix Gla protein	1.7	N/A	2.7	N/A	2.3	0.140	2.0	N/A	2.0	N/A	6.8	0.220
MIME_HUMAN	Mimecan							6.1	0.135	16.5	0.047	1.7	N/A
MMP2_HUMAN	72 kDa type IV collagenase	1.0	-	1.2	N/A	1.2	N/A						
MXRA5_HUMAN	Matrix-remodeling-associated protein 5	1.0	-	2.9	0.144	1.7	N/A	1.0	-	1.0	-	1.5	N/A

NID1_HUMAN	Nidogen-1‡	1.2	0.775	3.6	0.059	1.7	N/A	0.7	0.316	0.6	0.572	0.2	0.050
NID2_HUMAN	Nidogen-2							1.0	0.909	14.2	0.051	4.5	0.067
OSTF1_HUMAN	Osteoclast-stimulating factor 1							1.0	-	1.0	-	1.7	N/A
OSTP_PIG	Osteopontin	1.0	-	1.0	-	8.1	N/A	1.0	-	1.0	-	13.6	N/A
PA2GX_HUMAN	Group 10 secretory phospholipase A2	1.0	-	1.0	-	1.5	N/A						
PCOC1_HUMAN	Procollagen C-endopeptidase enhancer 1	1.0	-	1.0	-	4.5	0.030						
PF11_PIG	Prophenin-1 (Fragment)							0.4	0.174	1.4	0.611	0.8	0.814
PGBM_HUMAN	Basement membrane-specific heparan sulfate proteoglycan core protein	1.2	0.681	3.6	0.051	2.5	0.161	0.5	0.129	1.7	0.220	0.5	0.035
PGCA_HUMAN	Aggrecan core protein							1.0	-	1.7	N/A	34.0	0.008
PGS1_HUMAN	Biglycan							3.0	0.117	22.5	0.017	24.8	0.007
PGS2_PIG	Decorin	2.3	0.075	1.8	0.071	1.8	0.114	1.1	0.827	1.2	0.630	1.0	0.962
PODN_HUMAN	Podocan‡	1.0	-	3.0	0.143	2.3	0.140	1.0	-	1.0	-	1.9	N/A
POSTN_HUMAN	Periostin	1.4	N/A	3.7	0.057	3.6	0.038	1.7	N/A	9.9	0.003	19.5	0.039
PRELP_HUMAN	Prolargin‡	1.0	-	1.8	0.187	11.2	0.001*	1.5	0.143	2.9	0.035	2.9	0.114
SAMP_PIG	Serum amyloid P-component	1.0	-	1.7	N/A	3.7	0.047	1.0	-	1.0	-	3.3	N/A
SAP_HUMAN	Proactivator polypeptide	0.9	0.781	1.4	0.494	1.9	0.287	1.0	-	1.5	0.561	1.6	0.478
SFRP1_HUMAN	Secreted frizzled-related protein 1	1.0	-	1.0	-	1.5	N/A	1.0	-	1.0	-	2.7	N/A
SFRP3_HUMAN	Secreted frizzled-related protein 3	2.0	0.268	4.2	0.114	2.6	N/A						
SPON1_HUMAN	Spondin-1‡	2.0	0.078	8.5	<0.001*	11.6	0.012	2.7	0.032	1.5	N/A	1.0	-
SPP24_PIG	Secreted phosphoprotein 24	1.0	-	4.6	0.040	5.1	0.248	1.0	-	1.0	-	7.3	N/A
SPRC_HUMAN	SPARC	1.0	-	2.7	0.233	3.2	0.168	1.0	-	1.0	-	1.7	N/A
SSPO_HUMAN	SCO-spondin	1.0	-	1.2	N/A	1.3	N/A	1.0	0.971	1.0	-	1.0	-
TARSH_HUMAN	Target of Nesh-SH3							1.0	-	3.7	0.157	5.7	0.054
TENA_PIG	Tenascin	1.4	0.550	20.6	0.004	7.1	0.053	0.5	N/A	44.8	0.040	37.4	0.072
TENX_HUMAN	Tenascin-X‡	1.8	0.009	2.2	0.229	7.1	0.085	0.4	0.135	0.7	0.628	1.7	0.409
TETN_HUMAN	Tetranectin‡	2.1	0.079	1.7	0.004	2.8	0.027	2.4	0.156	5.8	0.008	6.7	0.038
THS7A_HUMAN	Thrombospondin type-1 domain-containing protein 7A							1.8	N/A	1.5	N/A	1.0	-
TIMP1_PIG	Metalloproteinase inhibitor 1	1.0	-	1.0	-	1.3	N/A						
TINAL_HUMAN	Tubulointerstitial nephritis antigen-like‡							2.7	0.137	6.8	0.078	0.3	N/A
TSP1_HUMAN	Thrombospondin-1	2.7	0.403	13.5	0.015	27.4	0.063	1.0	-	1.7	N/A	10.1	N/A
TSP4_HUMAN	Thrombospondin-4	3.6	0.099	21.3	0.005	15.6	0.003	1.0	-	3.7	0.156	6.6	0.124
VTNC_PIG	Vitronectin	2.5	0.179	1.8	0.035	3.8	<0.001*	1.9	0.422	26.4	0.109	33.2	0.323

P-values were derived from unpaired Student's t-tests with unequal variance (note that every time protein expression in the majority of samples from one of the two groups compared was undetectable, the t-test was not performed).

N/A denotes “non applicable”. False discovery rates (FDR) were calculated using the R-package QVALUE, *<5%; ‡, proteins that returned zero hits in a Pubmed query of title/abstracts in combination with any of the following terms: "myocardial infarction", "cardiac remodeling" or "ischemic remodeling".

Figure Legends:

Figure 1. Characterisation of I/R in the swine model. **A)** Echocardiography showing the characteristic loss of mass and absence of contraction in the LV anterior wall. **B)** Representative pig hearts 15 days and 60 days post I/R injury. Samples were taken for proteomic analysis at the specified locations. **C)** Masson's trichrome and hematoxyline & eosin staining in control and infarcted hearts. Magnification: 10x, scale bar: 200µm.

Figure 2. Distribution of ECM proteins. **A)** Electron microscopy image of decellularised cardiac tissue after 0.1% SDS treatment. Magnification: 10,000x, scale bar: 5µm **B)** The distribution of ECM proteins was compared in the NaCl and Guanidine-HCl extracts (GU) according to their biochemical (upper panels) and functional classification (lower panels). For each category, the number of identified proteins (n) is shown while the total spectral counts are depicted in the charts.

Figure 3. Differential expression of ECM proteins. Protein expression was compared between COR I/R15 and COR Ctrl **(A)**, LV I/R15 and LV Ctrl **(B)**, and LV I/R60 and LV Ctrl **(C)**. Each point represents an individual protein. Vertical lines represent 2-fold difference in levels; horizontal lines represent P=0.01. The most prominent differences (P<0.01 and fold changes >2 or <0.5) are labeled. See **Table 1** for a complete list of ECM proteins. Multiple two-group t tests were performed for LV samples (**B**, **C**) to be directly comparable with the analyses for COR samples (**A**).

Figure 4. Interactome of the cardiac ECM. Pathway Studio (Ariadne Genomics) was used to depict relevant interactions of the differentially expressed ECM proteins (**Figure 3**) with TGFb-1 and their relationship with "disease" (red boxes) or "cell processes" (orange boxes). Novel proteins in cardiac remodeling after I/R injury are highlighted with a blue halo.

Figure 5. Cardiac ECM remodelling. Principal component analysis based on all proteins identified in the NaCl **(A)** and Guanidine-HCl extracts **(B)**. Data points represent individual biological replicates (n=4 per group). Hierarchical clustering of the top 20 most differentially expressed proteins across groups (one-way ANOVA) in the NaCl **(C)** und Guanidine-HCl extracts **(D)**. Blue-red heat map values correspond to low-high protein expression levels. The boxed ECM proteins were selected for further validation.

Figure 6. Comparison of protein and gene expression. Real-time PCR for CILP1, asporin (ASPN), aortic carboxipeptidase-like protein (ACLP/AEBP1), BGH3, collagen alpha-1(XIV) (COEA1) and collagen alpha-1(XVIII) (COIA1) **(A)**. Normalized spectral counts for the corresponding proteins in the Guanidine-HCl **(B)** and the NaCl extracts **(C).** Results are shown as mean±SD, * denotes significant difference from controls, $P<0.05$. Scatter plots depict the correlation of mRNA levels **(D)** and protein levels **(E**, total spectral counts in Guanidine-HCl + NaCl extracts) in the focal lesion (LV) and the border zone (COR). Note that mRNA expression was highly correlated, but protein levels were markedly different in the two regions.

Figure 7. Role of TGFβ-1. **A)** Immunoblots confirming higher levels of asporin, ACLP/AEBP1, dermatopontin (DERM), biglycan (PGS1) and periostin (POSTN). Their upregulation co-incided

with a loss of the latency associated peptide-TGFβ-1 complex, which migrates at its characteristic molecular weight of approx. 40 kDa. Silver-stained images demonstrating equal loading are provided in **Supplemental Figure II**. **B)** Quantitation for latency associated peptide-TGFβ-1 complex by densitometry; *** P<0.001 **C)** Effects of TGFβ-1 and hypoxia on the expression of BGH3, dermatopontin, asporin and ACLP/AEBP-1 in cardiac fibroblasts (n=9, means and 95% confidence intervals). Two-way ANOVA was used to test for differences across treatment groups (control, TGFβ-1, hypoxia, TGFβ-1 and hypoxia) and time points of measurement (24h, 48h). Bonferroni post tests for multiple comparisons to controls are shown, *** P<0.001. **D)** Staining for periostin, BGH3, dermatopontin and ACLP / AEBP-1. Left panels show negative controls (staining with secondary antibodies only). Note the extracellular distribution of periostin but the intracellular localization of AEBP-1.

Figure 8. Comparison of porcine and human tissues. Positive staining for asporin, CILP1 and dermatopontin was detectable (FITC-labelled antibodies, green color) in porcine **(A)** and human hearts **(B)**. Human LV tissue was obtained from patients undergoing cardiac transplant surgery for ischemic cardiomyopathy or healthy organ donors. No staining was observed in non-ischemic controls (Ctrl). Vimentin staining (R-phycoerythrin, red color) was performed to visualize fibroblasts. Magnification: 40x, scale bar: 50μm.

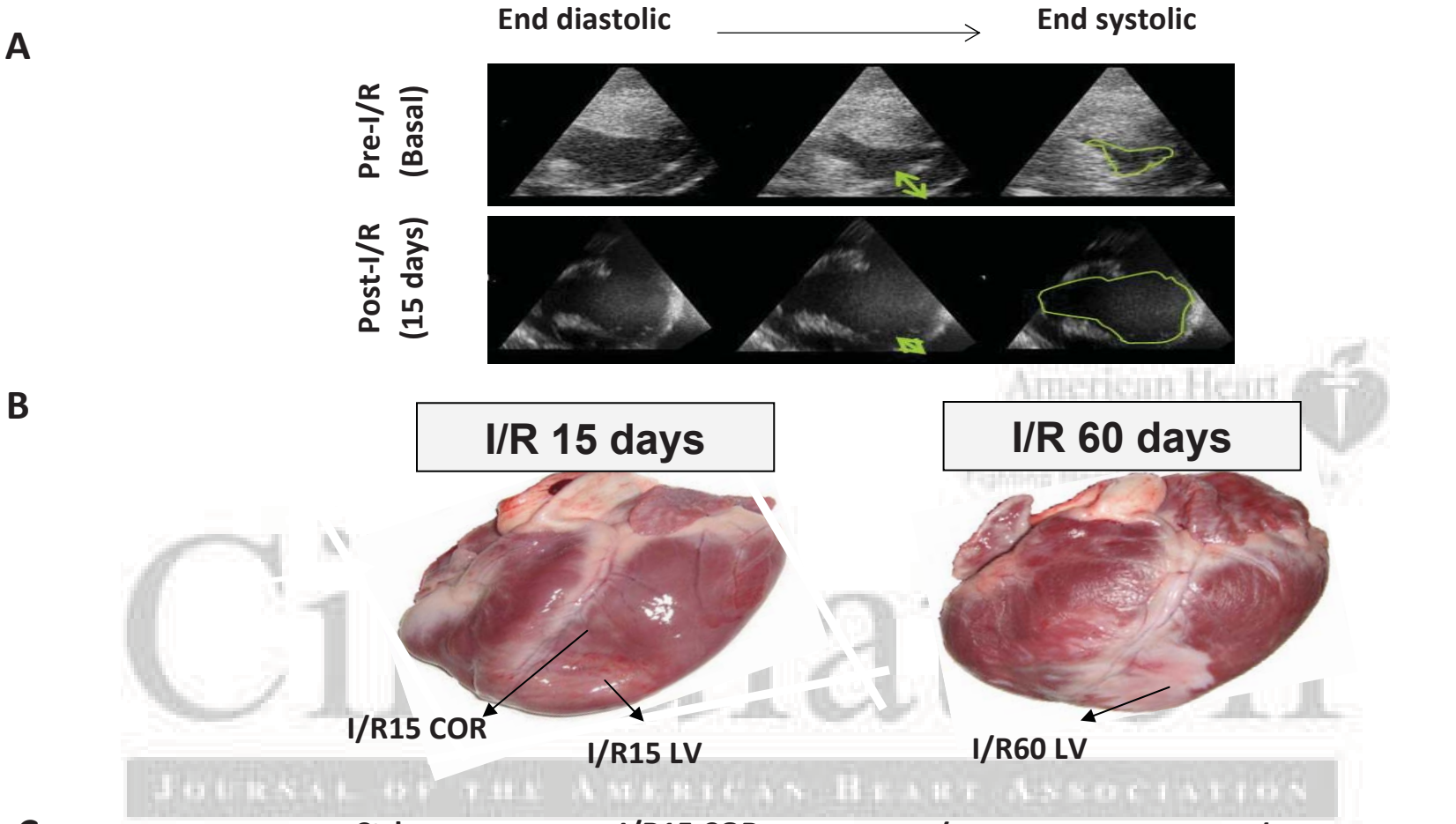
A
End diastolic
End systolic
Pre-I/R (Basal)
Post-I/R (15 days)
B
I/R 15 days
I/R 60 days
I/R15 COR
I/R15 LV
I/R60 LV
C
Ctrl
I/R15 COR
I/R15 LV
I/R60 LV
Masson's trichrome
Hematoxiline and eosine

A

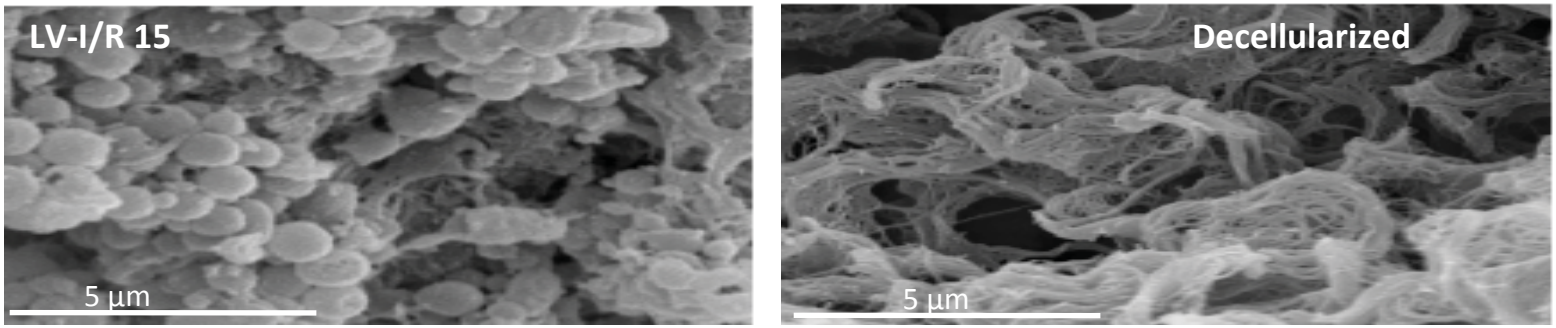
LV-I/R 15
5 µm
Decellularized
5 µm

B

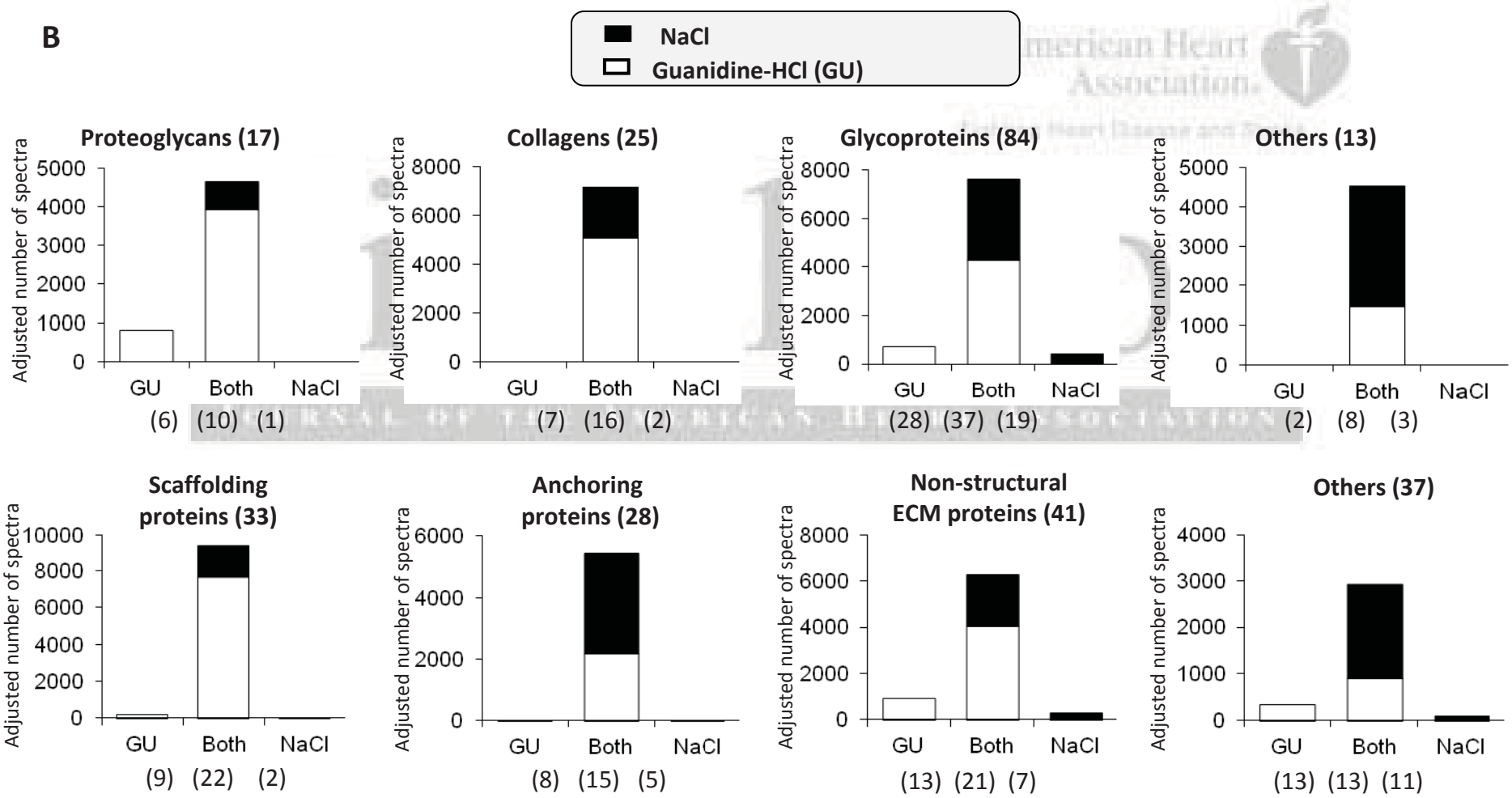
NaCl
Guanidine-HCl (GU)
Proteoglycans (17)
Collagens (25)
Glycoproteins (84)
Others (13)
Adjusted number of spectra
GU
Both
NaCl
(6) (10) (1)
(7) (16) (2)
(28) (37) (19)
(2) (8) (3)
Scaffolding proteins (33)
Anchoring proteins (28)
Non-structural ECM proteins (41)
Others (37)
(9) (22) (2)
(8) (15) (5)
(13) (21) (7)
(13) (13) (11)

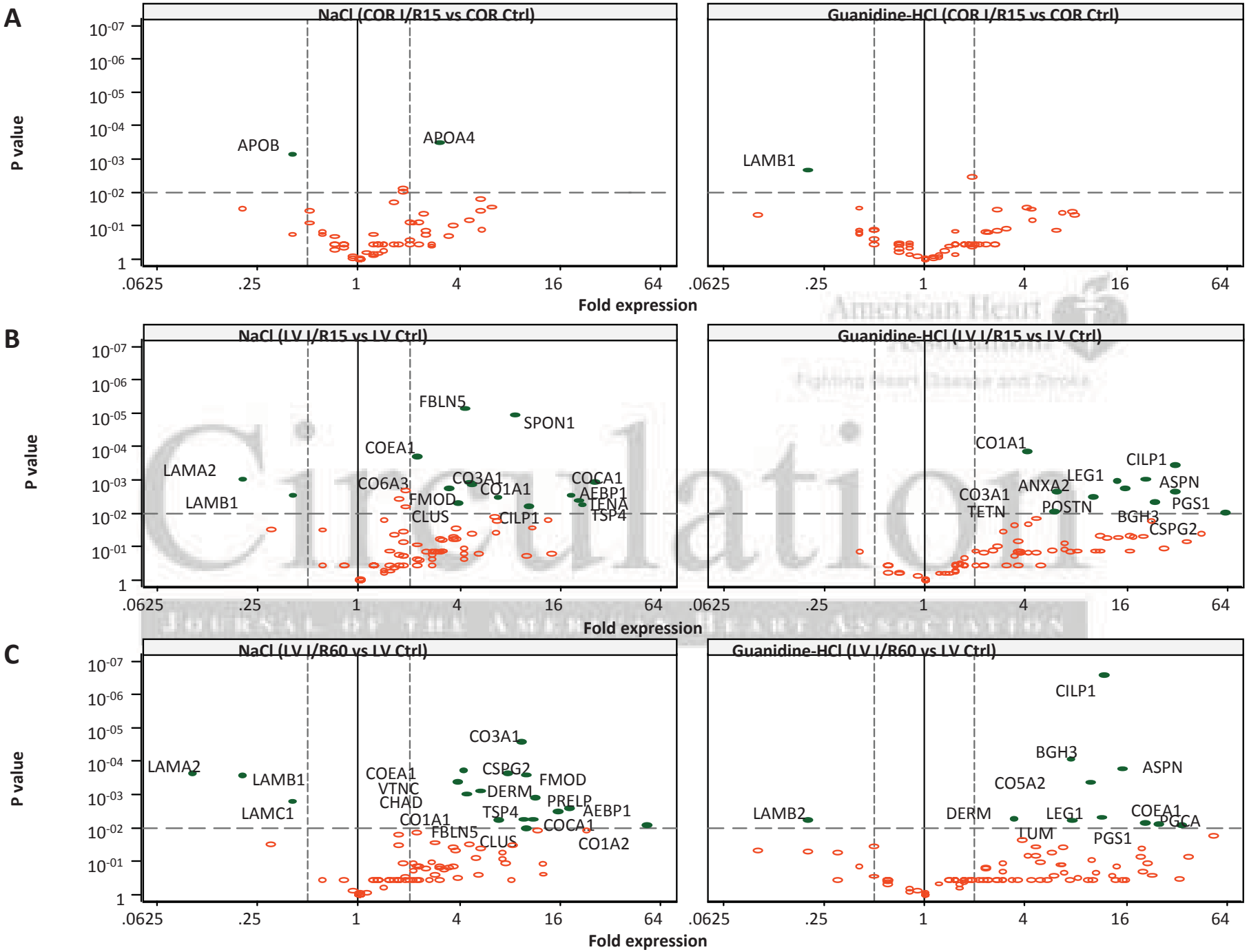
A
NaCl (COR I/R15 vs COR Ctrl)
Guanidine-HCl (COR I/R15 vs COR Ctrl)
P value
APOB
APOA4
LAMB1
Fold expression
B
NaCl (LV I/R15 vs LV Ctrl)
Guanidine-HCl (LV I/R15 vs LV Ctrl)
FBLN5
SPON1
COEA1
LAMA2
CO6A3
CO3A1
CO1A1
COCA1
AEBP1
TENA
TSP4
LAMB1
FMOD
CLUS
CILP1
CO1A1
CILP1
LEG1
ASPN
ANXA2
CO3A1
TETN
POSTN
PGS1
BGH3
CSPG2
Fold expression
C
NaCl (LV I/R60 vs LV Ctrl)
Guanidine-HCl (LV I/R60 vs LV Ctrl)
CO3A1
LAMA2
LAMB1
COEA1
CSPG2
FMOD
VTNC
DERM
CHAD
PRELP
LAMC1
TSP4
AEBP1
CO1A1
COCA1
FBLN5
CLUS
CO1A2
CILP1
BGH3
ASPN
CO5A2
LAMB2
DERM
LEG1
COEA1
PCOLCA
TUM
PGS1
Fold expression

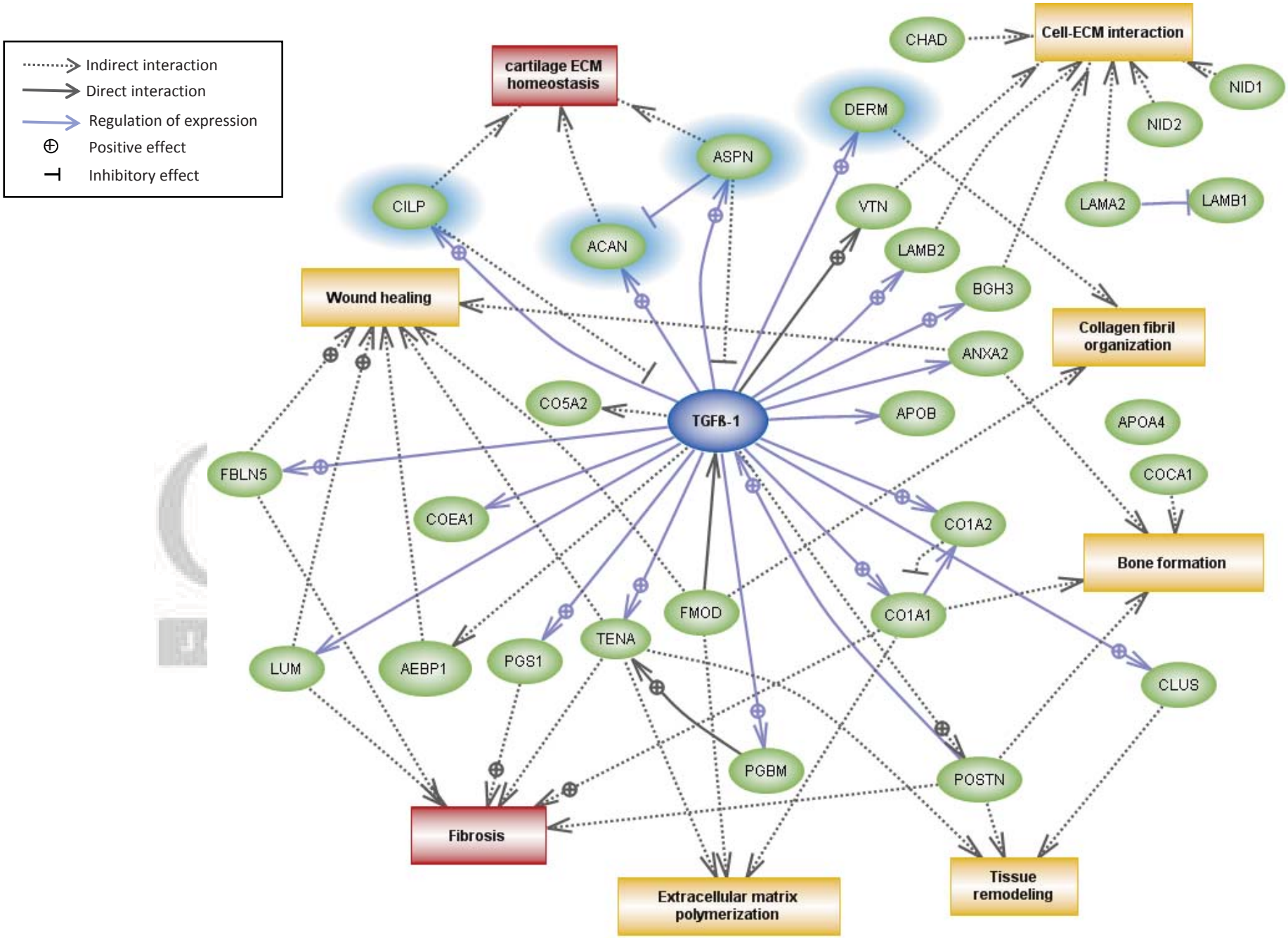
Indirect interaction
Direct interaction
Regulation of expression
Positive effect
Inhibitory effect
cartilage ECM homeostasis
CHAD
Cell-ECM interaction
NID1
NID2
DERM
ASPN
CILP
ACAN
VTN
LAMA2
LAMB1
LAMB2
Wound healing
BGH3
Collagen fibril organization
ANXA2
CO5A2
TGFß-1
APOB
APOA4
COCA1
FBLN5
COEA1
CO1A2
Bone formation
FMOD
CO1A1
TENA
LUM
AEBP1
PGS1
CLUS
PGBM
POSTN
Fibrosis
Extracellular matrix polymerization
Tissue remodeling

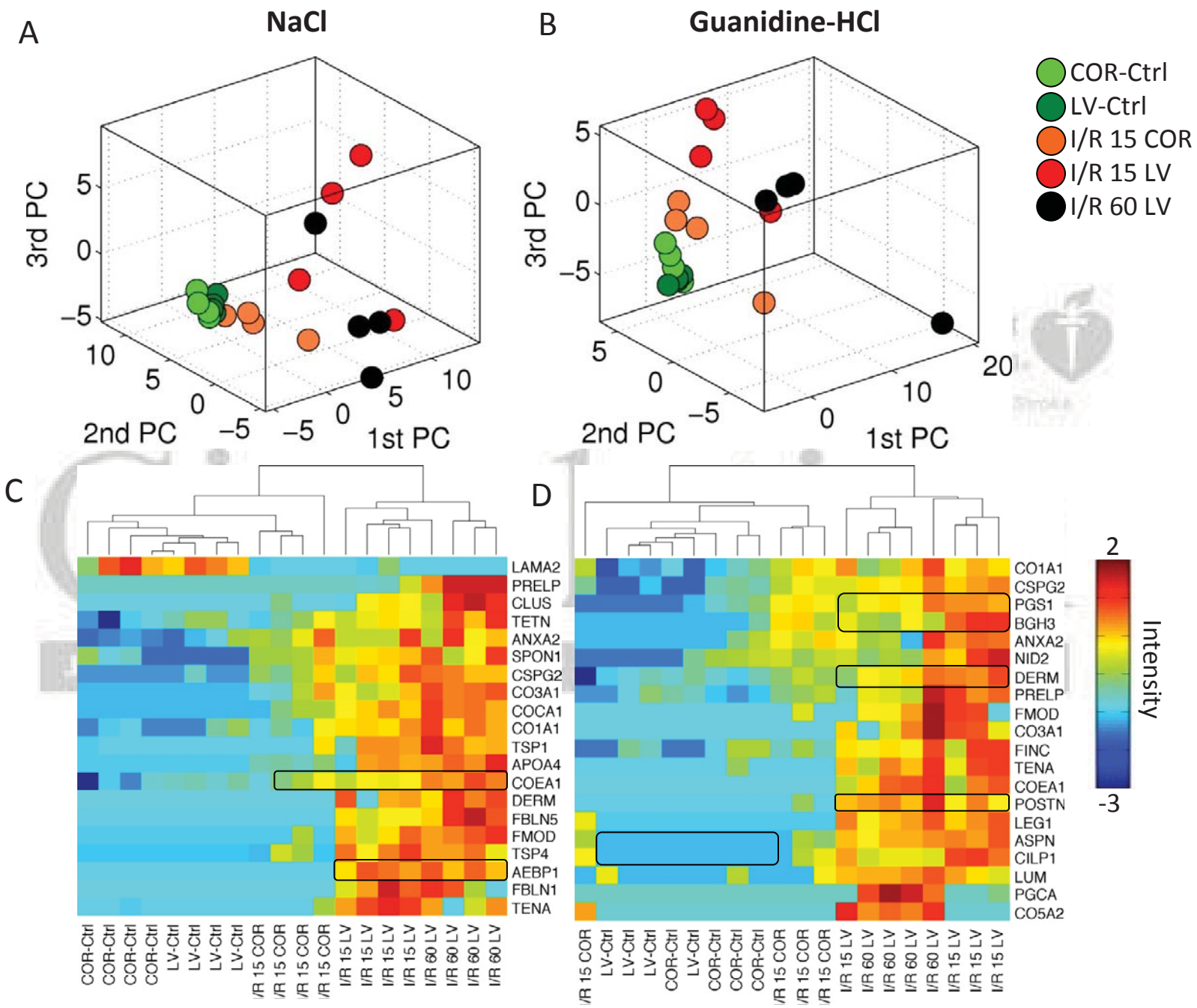
A
NaCl
B
Guanidine-HCl
COR-Ctrl
LV-Ctrl
I/R 15 COR
I/R 15 LV
I/R 60 LV
3rd PC
2nd PC
1st PC
C
D
LAMA2
PRELP
CLUS
TETN
ANXA2
SPON1
CSPG2
CO3A1
COCA1
CO1A1
TSP1
APOA4
COEA1
DERM
FBLN5
FMOD
TSP4
AEBP1
FBLN1
TENA
CO1A1
CSPG2
PGS1
BGH3
ANXA2
NID2
DERM
PRELP
FMOD
CO3A1
FINC
TENA
COEA1
POSTN
LEG1
ASPN
CILP1
LUM
PGCA
CO5A2
Intensity
2
-3

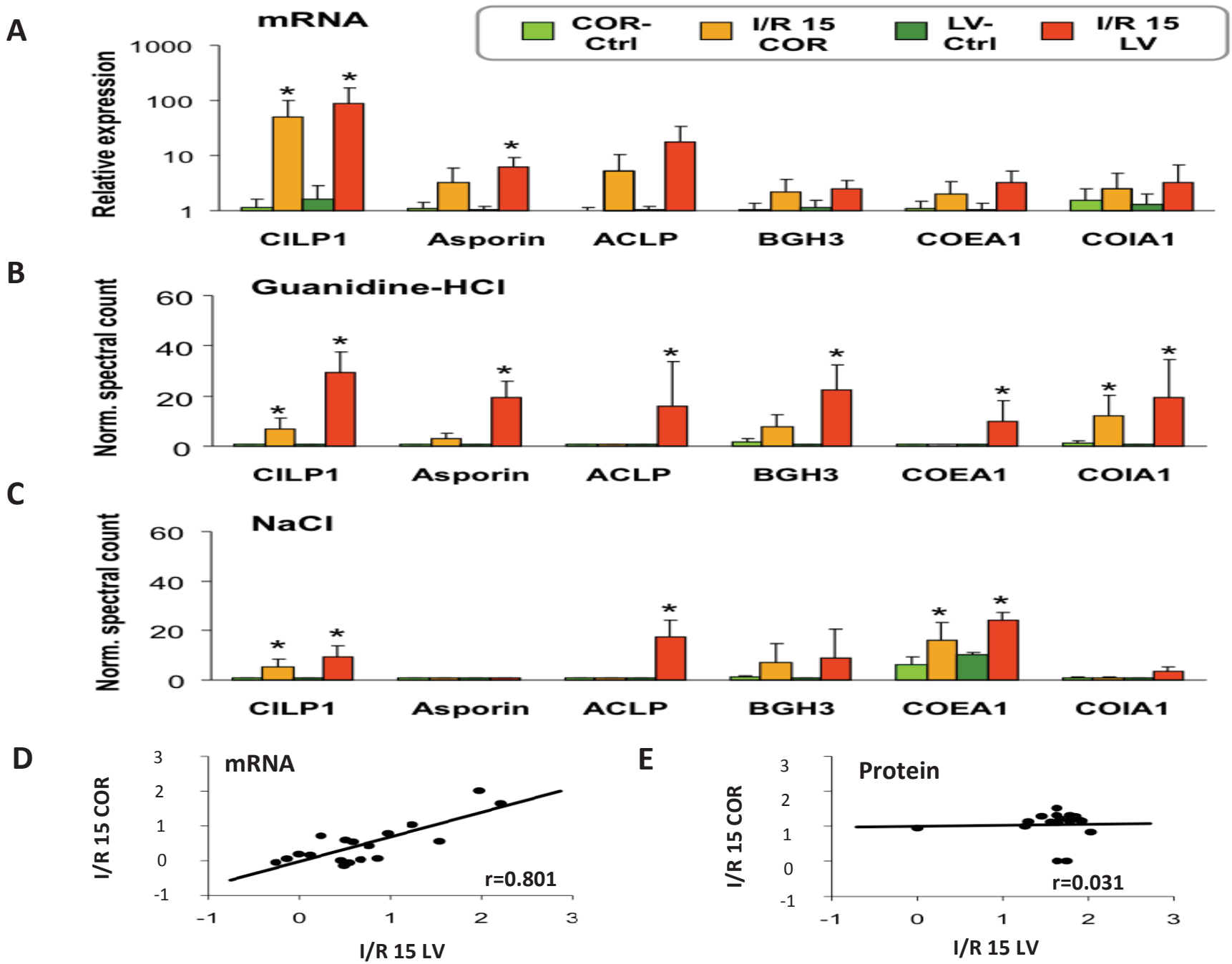
A
mRNA
COR-Ctrl
I/R 15 COR
LV-Ctrl
I/R 15 LV
Relative expression
1000
100
10
1
CILP1
Asporin
ACLP
BGH3
COEA1
COIA1
B
Guanidine-HCl
Norm. spectral count
60
40
20
0
CILP1
Asporin
ACLP
BGH3
COEA1
COIA1
C
NaCl
Norm. spectral count
60
40
20
0
CILP1
Asporin
ACLP
BGH3
COEA1
COIA1
D
mRNA
I/R 15 COR
I/R 15 LV
r=0.801
3
2
1
0
-1
-1
0
1
2
3
E
Protein
I/R 15 COR
I/R 15 LV
r=0.031
3
2
1
0
-1
-1
0
1
2
3

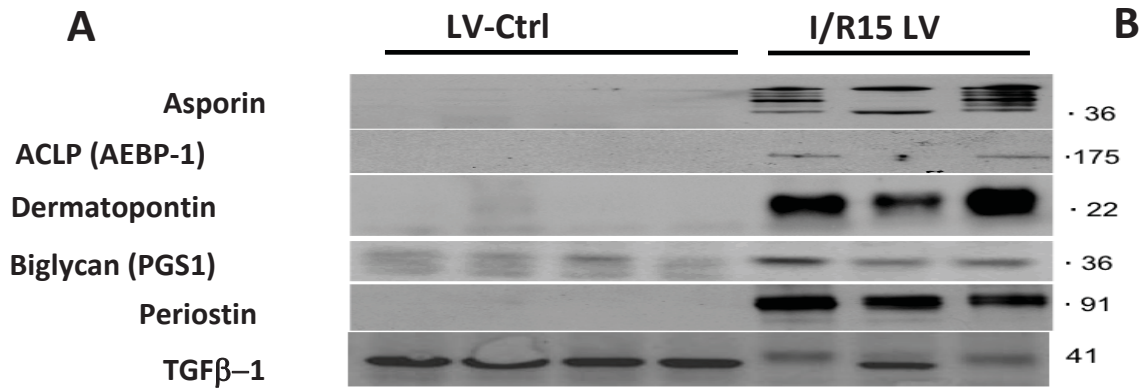
A
LV-Ctrl
I/R15 LV
Asporin
ACLP (AEBP-1)
Dermatopontin
Biglycan (PGS1)
Periostin
TGFβ–1
36
175
22
36
91
41

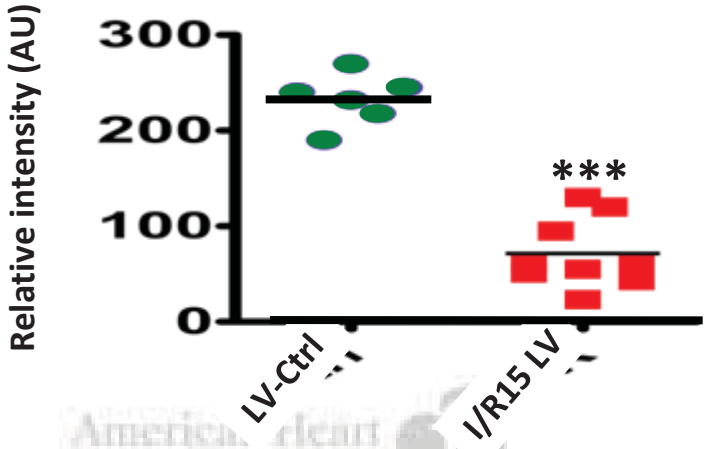
B
Relative intensity (AU)
300
200
100
0
***
LV-Ctrl
I/R15 LV

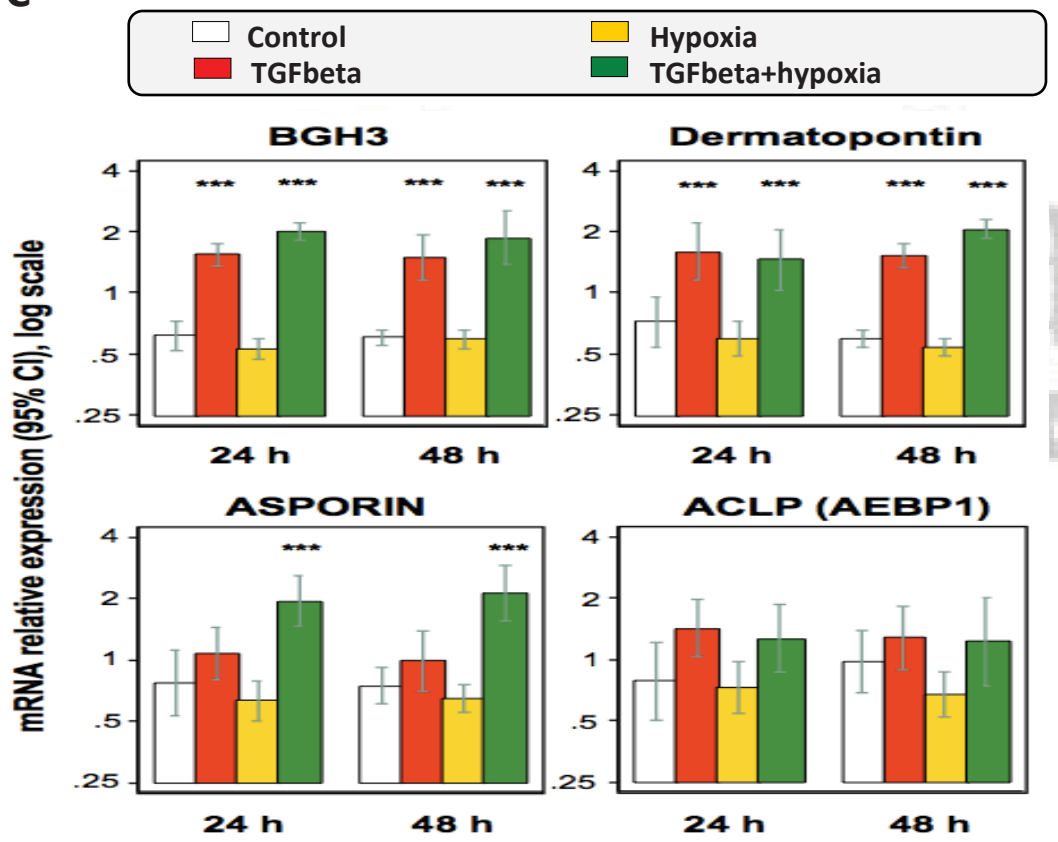
C
Control
TGFbeta
Hypoxia
TGFbeta+hypoxia
BGH3
Dermatopontin
ASPORIN
ACLP (AEBP1)
mRNA relative expression (95% CI), log scale
4
2
1
.5
.25
***
24 h
48 h

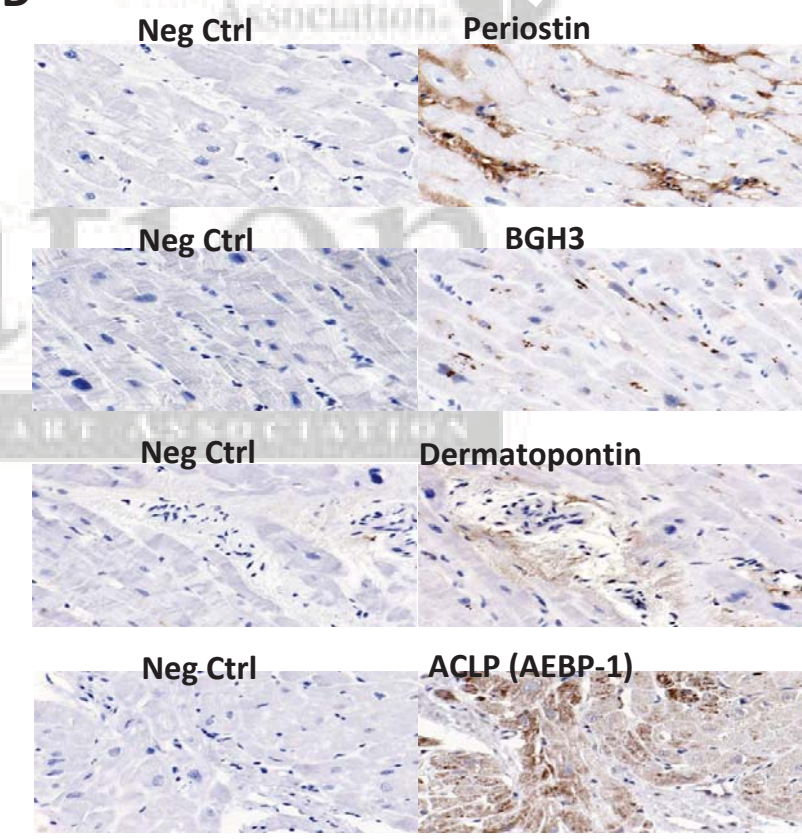
D
Neg Ctrl
Periostin
Neg Ctrl
BGH3
Neg Ctrl
Dermatopontin
Neg Ctrl
ACLP (AEBP-1)

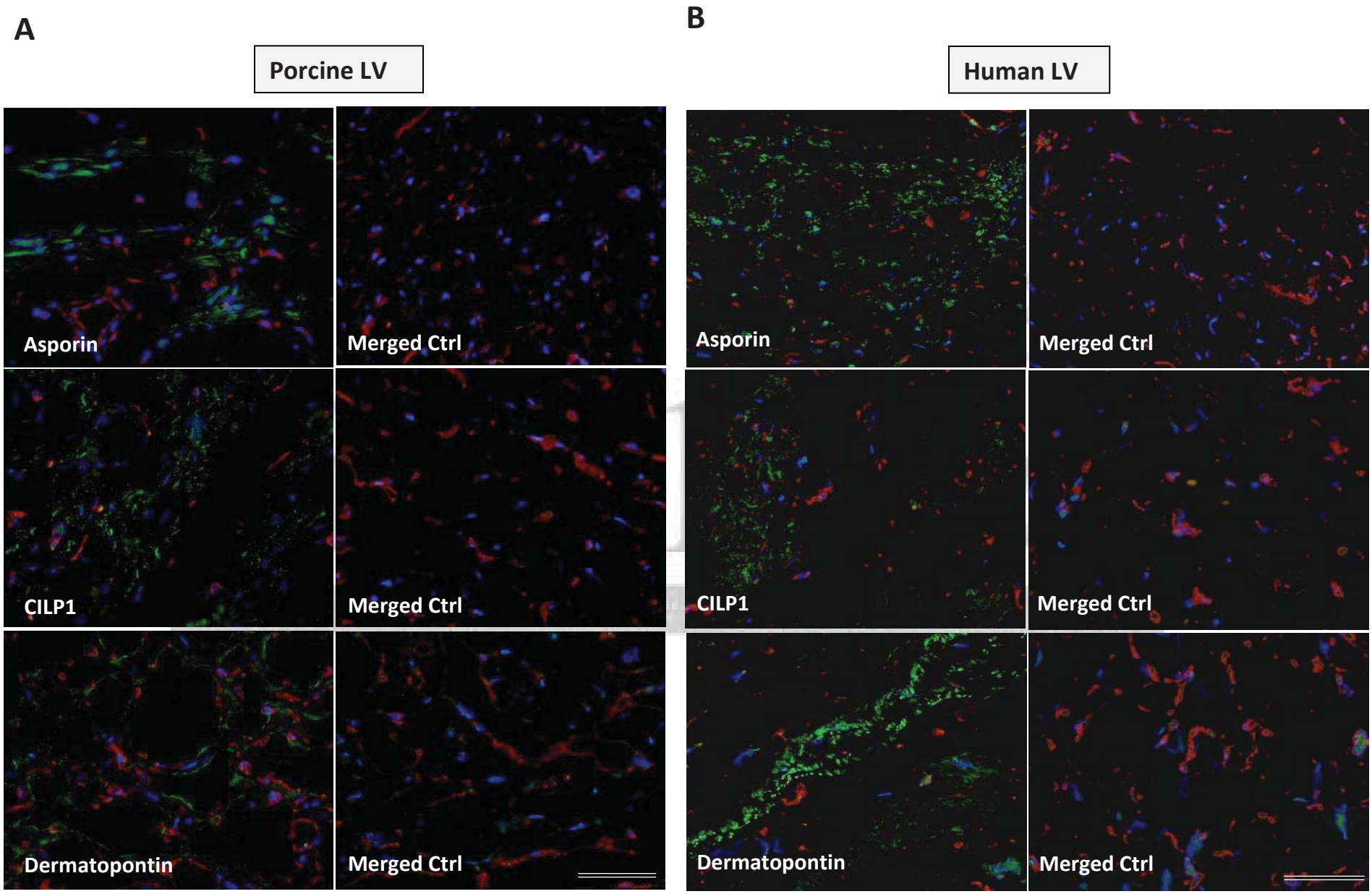
A
Porcine LV
Asporin
Merged Ctrl
CILP1
Merged Ctrl
Dermatopontin
Merged Ctrl
B
Human LV
Asporin
Merged Ctrl
CILP1
Merged Ctrl
Dermatopontin
Merged Ctrl